PORT SAID ENGINEERING JOURNAL
Faculty of Engineering - Port Said University
Volume 25 No. 2 September 2021 pp. 120 - 134
-Electrical Engineering-

SPLIE: Optimal Illumination Estimation for Structure Preserving Low-light Image Enhancement

Ghada Sandoub[1], Randa Atta[2], Hesham Arafat Ali[3], Rabab Farouk Abdel-Kader[4]

ABSTRACT

The images taken in low-light conditions often have many flaws such as, color vividness and low visibility which negatively affects the performance of many vision-based systems. Many of the existing Retinex-based enhancement algorithms improve the visibility of low-light images via estimating the illumination map and use it to obtain the corresponding reflectance. However, the improper estimation of the initial illumination map may produce unsatisfactory illuminated enhanced images with weak color constancy. To address this problem, this paper proposes an efficient algorithm for the enhancement of low-light images. In this algorithm, the initial illumination map is obtained by the fusion between the maximum color channel and bright channel prior. The estimated initial illumination map is then refined using a multi-objective problem that contains the illumination regularization terms specifically, the structural and textural details of the illumination. The optimization problem is solved using the alternative direction minimization (ADM) technique with the augmented Lagrangian multiplier to produce structure-aware smoothness of the initial illumination map. Finally, the contrast of the refined illumination map is adjusted using the gamma correction method. Experimental results on several benchmark datasets reveal the superiority of the proposed algorithm on the state-of-the-art algorithms in terms of qualitative and quantitative analysis. Furthermore, the proposed algorithm produces enhanced images with reducing the artifacts and preserving the naturalness and structural details.

Keywords: Image enhancement, Low-light image, Illumination estimation, Optimization

1. INTRODUCTION

Computer vision-based applications are designed for high-visibility input images. Contrariwise, images taken in low-light environments often have many flows, such as color vividness, low contrast, and low visibility of object details, due to inadequate or varying illumination. As these degradations affect the performance of vision-based applications, it is necessary to improve the low-light images visibility. Thus, many enhancement methods have been proposed in literature. Some of them improve the low-light image visibility by estimating its illumination component. However, the inaccurate estimation of the illumination component may result in color distortion, halo artifacts, and over-enhancement problems.

To address the drawbacks of current enhancement algorithms, an effective algorithm for low-light image enhancement is proposed through this paper. First, the initial illumination map is estimated by the fusion between maximum color channel and bright channel prior of input image to reduce the color distortion and halo artifacts problems produced from these channels.
Then, an optimal refinement is applied on initial illumination map using a multi-objective optimization problem. The optimal refinement provides structure-aware smoothing for the initial illumination map. Finally, the reflectance component which represents the enhanced image is retrieved by an element-wise division of input image by refined illumination based on Retinex model. The experimental results demonstrate that the proposed algorithm increase the visibility of low-light images and obtains natural results while preserving the structural details of enhanced images in comparison to several state-of-the-art algorithms.

The rest of the paper is organized as follows: In Section 2, the related work is reviewed. Section 3 includes the details of the proposed algorithm. The experimental results are given and analyzed in Section 4. Finally, Section 5 gives the paper conclusion.

2. RELATED WORK

Many image enhancement approaches have been introduced to enhance the brightness of low-light images,

[1]*Department of Electrical Engineering, Faculty of Engineering, PortSaid University, Egypt,email: ghadasandoub@eng.psu.edu.eg, Corresponding Author*

[2]*Department of Electrical Engineering, Faculty of Engineering, Port Said University, Egypt, email: r.atta@eng.psu.edu.eg*

[3]*Department of Computer Engineering and Systems, Faculty of Engineering, Mansoura University, Egypt, email: h_arafat_ali@mans.edu.eg*

[4]*Department of Electrical Engineering, Faculty of Engineering, Port Said University, Egypt, email: rababfakader@eng.psu.edu.eg*

Received: 03-05-2021, Accepted: 13-06-2021
DOI: 10.21608/PSERJ.2021.69512.1104

including histogram-based [1-8], deep learning-based [9-16], and Retinex-based methods [18-37]. The simplest and more intuitive way to improve the visibility of weakly illuminated images is to increase their brightness. Nevertheless, the saturation of bright regions during this operation may cause details loss. To avoid the above problem, histogram equalization (HE) methods [1], [2] were proposed in which the input image dynamic range is expanded. However, these methods are concerned with contrast enhancement rather than illumination adjustment which may result in under- or over-enhancement. To enhance the efficiency of HE methods, variational methods such as contextual and variational contrast enhancement (CVCE) [3] have been proposed. However, the variational methods concentrate on improving the illumination of low-light images while not considering the sharpness refinement. In [4], an exposure-based sub-image histogram equalization (ESIHE) was proposed. Through this method, the histogram is divided into a set of sub-histograms before performing equalizations using an exposure threshold to avoid over-enhancement. Nevertheless, this method enhances the local contrast only. Parihar and Verma [5] proposed an entropy based dynamic sub-histogram equalization (EDSHE) algorithm in which a recursive histogram division is performed depending on the entropy of sub-histograms. In [6], an enhancement algorithm was proposed to improve the visibility of low-light images based on gamma correction and histogram equalization. Furthermore, Tan and Isa [7] introduced an adjusted HE enhancement algorithm which segments the original histogram into sub-histograms using histogram segmentation thresholds based on exposure regions. In [8], an enhancement algorithm was proposed depending on quasi-symmetric correction (QCFs) and histogram equalization. It combines the locally-enhanced image and the globally-enhanced image performed via contrast limited adaptive histogram equalization (CLAHE) [1] and QCFs, respectively. Although HE-based methods enhance the contrast of low-light images, these methods suffer from over-enhancement. Further, they neglect the intensive noise in low-light images, especially in dark regions.

Recently, many algorithms based on deep-learning have been developed to address the problem of low-light image enhancement. In [9], a global illumination-aware and detail preserving network (GLADNet) was proposed. This method obtains the global illumination of input image using encoder-decoder network. In [10], LightenNet was proposed to predict the illumination map of a weakly illuminated image. However, this method fails to brighten low-light images that contain intensive noise. Wei et al. [11] introduced a deep Retinex-Net which consists of Decom-Net and Enhance-Net used for reflectance and illumination decomposition and illumination adjustment, respectively. In [12], a new network was proposed to enhance underexposed images based on learning an image-to-illumination rather than image-to-image mapping. However, this method may generate visual artifacts and color inconsistency when processing real-world images with various illumination intensities. In [13], unpaired learning framework called EnlightenGAN was proposed to train low-light enhancement model. In [14], a deep hybrid network was proposed based on learning the global content of weakly illuminated image using an encoder-decoder network and refining the edge details by using an improved spatially variant recurrent neural network (RNN). However, this method fails to brighten all dark regions. Ma et al. [15] proposed a context-sensitive decomposition network (CSDNet) architecture to exploit the scene-level contextual dependencies on spatial scales. In [16], a zero-reference deep curve estimation (Zero-DCE) algorithm was proposed based on a group of non-reference loss functions. Nevertheless, this method does not sufficiently enhance low-light images and suffers from color deviation. In general, the deep learning-based algorithms develop the performance of low-light image enhancement. However, they still suffer from some challenges, such as amplifying noise and color distortion. Furthermore, most of these algorithms are based on supervised learning which require large amount of training pairs of low/normal-light images. Thus, it is costly to prepare a large dataset. In addition, the constraints of training phase are complicated.

Many enhancement algorithms based on Retinex model have been proposed in literature. According to Retinex theory [17], the observed image is measured via the product of illumination and reflectance components. The conventional Retinex-based methods including, single scale Retinex (SSR) [18], multi-scale Retinex (MSR) [19], and MSR with color restoration (MSRCR) [20] use Gaussian filtering to obtain the illumination component of input image and consider the reflectance component as the final enhanced image. However, these algorithms suffer from over-enhancement, color distortion, and the enhanced image often looks unnatural. To address this problem, many variational Retinex-models have been proposed [21- 27]. These models obtain the enhanced image depending on the simultaneous estimation of reflectance and illumination components. In [21], a variational Retinex framework was proposed using bright channel prior. However, the enhanced images produced from this method suffer from amplified noise and halo artifacts around edges. In [22], a weighted variational method was introduced to simultaneously obtain the reflectance and illumination components from the observed image. However, this method fails to improve the illumination of dark regions in weakly illuminated images. Wu et al. [23] introduced an enhancement algorithm depending on an image degradation model. However, this method does not take into consideration the intensive noise in dark regions and its results are visually unpleasant. In [24], a robust Retinex model was proposed with an additional noise term to reduce the amount of noise in the enhanced images. Nevertheless, this method suffers from over smoothing in some regions which

results in a degraded image due to the loss of its details. Furthermore, in [25], an enhancement algorithm was proposed depending on separating the illumination and reflectance components while suppressing the intensive noise. In addition, this method contains post-processing algorithms which correct the color distortion in illumination component and enhance the reflectance component contrast. In [26], an optimization framework was introduced to obtain a smoothed illumination component and a noise-suppressed reflectance component. Nevertheless, this method suffers from halo artifacts on the boundaries besides the high complexity. Furthermore, Wang et al. [27], proposed a structure-based low-rank Retinex model for simultaneous low-light image enhancement and noise removal. In general, the simultaneous estimation of the reflectance and illumination components from a single image is an ill-posed problem which makes the complexity of these algorithms very high. Therefore, these algorithms are not suitable for real-time applications.

Another set of Retinex-based algorithms was proposed to make the low-light images more visible based on the estimation of illumination component which used to recover the reflectance component. Zheng et al. [28], introduced a naturalness preserved enhancement (NPE) algorithm to improve the contrast of non-uniform illumination images. This method used the bright-pass filter to estimate the illumination component which is then adapted using a bi-log transformation. The NPE algorithm produces promising results while preserving the naturalness. Nevertheless, it suffers from high computational cost. In [29], the bright channel prior was used to estimate the illumination map of input images. However, the enhanced images produced by this method may contain noise and halo artifacts. Furthermore, Chen et al. [30] introduced an enhancement algorithm for low-light images based on maximum color channel in which the maximum value among R, G, and B channels of the observed image is obtained to estimate the illumination. Although this method does not cause halo artifacts, it results in color distortion in the enhanced image. In [31], a fusion-based algorithm was proposed to enhance the brightness of weakly-illuminated images. This method adjusts the illumination of input image via fusing several derivatives of the illumination map that was initially estimated. Li et al. [32] proposed a low-light image enhancement (LIME) algorithm. It gets the initial illumination map of input image via seeking for the maximum value among its R, G, and B channels and then the illumination map is refined using smoothing model. Although this method increases the global brightness, some regions in the enhanced image suffer from over-enhancement and often have amplified noise buried in dark regions. In [33], a camera response model was adopted to brighten the single image by adjusting each pixel to the desired exposure. Nevertheless, the enhanced image produced by this method may contain visual artifacts. In [34], a non-uniform illumination prior model was proposed to enhance the visibility of low-light images. Furthermore, Zhang et al. [35] proposed a dual illumination estimation algorithm to simultaneously handle both overexposed and underexposed images. However, this method fails to recover vivid textures of overexposed images. In [36], an image enhancement method performing a structure-aware estimation of the initial illumination was proposed. Then, a multi-objective optimization function is minimized to refine the illumination estimation. Furthermore, Feng et al. [37] proposed a low-light image enhancement algorithm based on multi-illumination estimation in which multiple exposure correction images are obtained. The Laplacian multi-scale fusion is then used to combine the estimated weight map and the images with different degrees of exposure. Broadly speaking, the improper estimation of illumination component may result in a degraded image. Therefore, this type of algorithms requires an accurate illumination estimation scheme to produce visually pleasing results.

3. STRUCTURE PRESERVING LOW-LIGHT IMAGE ENHANCEMENT (SPLIE)

As shown in Figure 1, the proposed SPLIE algorithm is divided into two stages. The first stage includes the estimation of initial illumination map using fusion-based bright channel. Then, the illumination map is refined based on minimizing multi-objective function to obtain the enhanced result. The stages of the proposed SPLIE algorithm are demonstrated in details in the following sub-sections.

3.1. Initial Illumination Map Estimation

According to Retinex theory [17], the low-light image is composed of the illumination and reflectance components as follows:

$$\boldsymbol{I} = \boldsymbol{L} \circ \boldsymbol{R}, \tag{1}$$

where the operator $\circ$ denotes the element-wise multiplication, and $\boldsymbol{I}$, $\boldsymbol{L}$, and $\boldsymbol{R}$ represent the input image, the illumination map, and the scene reflectance, respectively. When estimating the illumination $\boldsymbol{L}$ of the low-light image $\boldsymbol{I}$, the scene reflectance $\boldsymbol{R}$ which represents the enhanced image can be obtained as:

$$\boldsymbol{R} = \boldsymbol{I} \oslash \boldsymbol{L}, \tag{2}$$

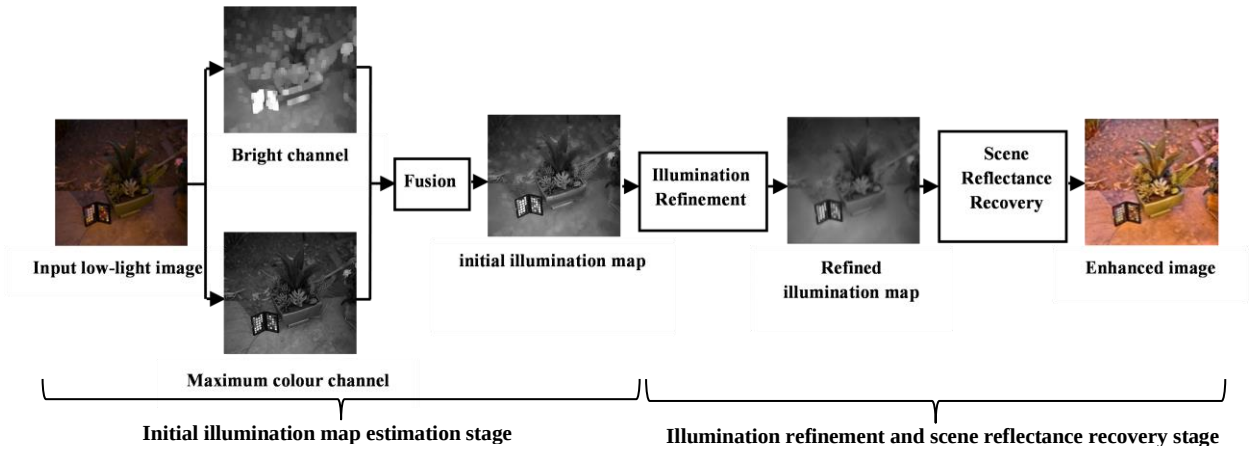

Figure 1: The stages of the proposed structure preserving low-light image enhancement (SPLIE) algorithm

where the operator ⊘ represents the element-wise division. The way of estimating the illumination map $\boldsymbol{L}$ plays an important rule in the recovery of scene reflectance $\boldsymbol{R}$ and the improper estimation of the illumination map may result in a degraded image. Therefore, the goal of this paper is obtaining the optimal illumination map.

There are several methods for estimating the initial illumination map $\hat{\boldsymbol{L}}$. Max-RGB [30], [38] is a method of color constancy in which the illumination map is estimated via looking at each location x in the input image for the maximum value among the RGB color channels as follows:

$$\hat{L}_{max}(x) = \max_{c\in\{R,G,B\}}(I^c(x)). \quad (3)$$

This method can boost the global illumination. However, it does not take into account the neighbouring pixels in the enhanced image which may lead to the color distortion. To enhance the performance of the above method, another method has been introduced to estimate the illumination using the bright channel prior in which the illumination is obtained by considering the neighbours of the current pixel in a small region [20]. The bright channel of a weakly illuminated input image is written as:

$$\hat{L}_{bright}(x) = \max_{c\in\{R,G,B\}}(\max_{y\in\Omega(x)} I^c(y)), \quad (4)$$

where $\Omega(x)$ denotes the local patch centred at x having size of $w \times w$ (w = 15 is chosen in this paper). The bright channel is obtained by determining each color channel's maximum value through each patch $\Omega(x)$. Then, the maximum value among the RGB color channels is estimated. Although the local consistency is improved by using the methods that based on bright channel prior, they result in halo artifacts especially when using a large patch size. In the case of 1×1 patch size, the bright channel prior has similar effect as the maximum color channel. Therefore, both channels have no halo artifacts but result in color distortion. Many algorithms [32, 36] have used the bright channel or its improvement as initial illumination. However, the bright channel may not represent true illumination as it does not distinguish the illumination of the adjacent objects in the low-light image.

Therefore, to overcome these mentioned problems, an initial illumination map estimation algorithm is proposed to provide near actual estimation of the illumination map of low-light images. The initial illumination of low-light image in the proposed algorithm is obtained based on the fusion of both the maximum color and bright channels to reduce the color distortion and the halo artifacts problems produced from both channels [39]. First, Gaussian filter [40] is applied to the bright channel ($\hat{\boldsymbol{L}}_{bright}$) to smoothen its halo artifacts. The fusion of the maximum color channel $\hat{L}_{\max}$ with the bright channel $\hat{L}_{\text{bright}}$ is then done by estimating a weight which represents the halo strength at each pixel in the bright channel. It is estimated based on the normalized difference between both channels as follows:

$$W(x) = (\hat{L}_{bright}(x) - \hat{L}_{max}(x))/\hat{L}_{bright}(x), \quad (5)$$

where the value of $W(x)$ has a range of [0,1]. According to the weight value at each pixel, the fusion-based initial illumination algorithm accurately estimates the illumination map by calculating the sum of maximum color channel $\hat{\boldsymbol{L}}_{max}$ and bright channel $\hat{\boldsymbol{L}}_{bright}$ based on the estimated weight as:

$$\hat{L}(x) = \hat{L}_{bright}(x) \cdot (1 - W(x)) + \hat{L}_{max} \cdot W(x). \quad (6)$$

According to (6), when the weight takes a value close to 1 which indicates that the halo artifacts are strong, the illumination component is obtained via providing larger weight to $\hat{\boldsymbol{L}}_{max}$ while providing $\hat{\boldsymbol{L}}_{bright}$ with less weight and vice versa.

The halo artifacts at the edge pixels are strong in which the weight will take a value near to 1. Therefore, according to (6) more weight is provided to $\hat{\boldsymbol{L}}_{max}$ and less weight is provided to $\hat{L}_{bright}(x)$ to obtain the illumination component. Therefore, the results produced by the fusion-based mechanism in this case are mostly similar to the results of maximum color channel in which the enhanced images have no halo artifacts. Contrariwise, although the homogeneous regions are clear from any halo artifacts, a color distortion may appear at these regions. Hence, the results produced by the fusion-based mechanism are mostly the same as the results generated from the bright channel prior. Consequently, the proposed fusion-based mechanism weakens the color distortion and halo artifacts in the estimated illumination.

3.2. Illumination Refinement and Image Enhancement

Although the proposed initial illumination $\hat{\boldsymbol{L}}$ shown in Figure 2 (b) provides a good estimation of actual illumination of input images, the estimated illumination map may contain some textural details which leads to over-enhanced images.

In this case, the initial illumination map should be refined in order to smoothen the textural details and preserve the overall structural details of the image. Thus, the structure-aware smoothness of the initial illumination map is performed using the following optimization problem [36]:

$$\min_{\boldsymbol{L}} \|\hat{\boldsymbol{L}} - \boldsymbol{L}\|_2^2 + \alpha\|\nabla \boldsymbol{I}_m - \nabla \boldsymbol{L}\|_2^2 + \beta\|\boldsymbol{T} \circ \nabla \boldsymbol{L}\|_1, \quad (7)$$

where $\hat{\boldsymbol{L}}$ and $\boldsymbol{L}$ are the initial illumination obtained by (6) and the refined illumination, respectively. ∇ denotes the gradient operator, $\boldsymbol{T}$ is the weight matrix, $\nabla \boldsymbol{I}_m$ represents maximum of ∇ from all channels of low-light image $\boldsymbol{I}$. Further, α and β are the regularization parameters which balance the involved terms, $\|\,.\,\|_2$ and $\|\,.\,\|_1$ represent the l_2 and l_1 norms, respectively. In (7), the first term represents the fidelity between the initial and the refined illumination maps. In order to maintain the illumination map's structural details, the second term of (7) makes the gradient of the refined illumination $\nabla \boldsymbol{L}$ closer to the maximum gradient of input mage $\nabla \boldsymbol{I}_m$, while the third term considers the smoothness of textural details. Using the second and third terms of (7) provides the balance between preserving structural details, and smoothening textural details in the illumination map and thus produces structure-aware smoothness of the illumination map.

For the textural details smoothing, the weight matrix $\boldsymbol{T}$ is calculated depending on the initial illumination map $\hat{\boldsymbol{L}}$ using the relative total variation [41]. It is estimated for each location as follows:

$$T_h = \sum_{y \in \Omega(x)} \frac{G_\sigma(x,y)}{|\sum_{y \in \Omega(x)} G_\sigma(x,y) \nabla_h \hat{L}(y)| + \varepsilon};$$

$$T_v = \sum_{y \in \Omega(x)} \frac{G_\sigma(x,y)}{|\sum_{y \in \Omega(x)} G_\sigma(x,y) \nabla_v \hat{L}(y)| + \varepsilon}, \quad (8)$$

where the symbols ∇_v and ∇_h represent the first order derivatives over the vertical and horizontal directions, respectively. $G_\sigma(x,y)$ denotes the Gaussian kernel with standard deviation σ and it is given by:

$$G_\sigma(x,y) \propto exp(-\tfrac{\|x-y\|^2}{2\sigma^2}). \quad (9)$$

The optimization problem (7) can be efficiently solved by using the alternative direction minimization (ADM) technique [42]. To make the problem separable for easy solving, the term $\nabla \boldsymbol{L}$ is replaced with an auxiliary variable $\boldsymbol{M}$. Consequently, the optimization problem is formulated as:

$$\min_{\boldsymbol{L},\boldsymbol{M}} \|\hat{\boldsymbol{L}} - \boldsymbol{L}\|_2^2 + \alpha\|\nabla \boldsymbol{I}_m - \boldsymbol{M}\|_2^2 + \beta\|\boldsymbol{T} \circ \boldsymbol{M}\|_1$$
$$s.t.\ \nabla \boldsymbol{L} = \boldsymbol{M} \quad (10)$$

This constrained optimization problem can be solved using the augmented Lagrangian multiplier method and converted into its equivalent unconstrained form as:

$$\mathcal{L} = \|\hat{\boldsymbol{L}} - \boldsymbol{L}\|_2^2 + \alpha\|\nabla \boldsymbol{I}_m - \boldsymbol{M}\|_2^2 + \beta\|\boldsymbol{T} \circ \boldsymbol{M}\|_1 + \Phi(\boldsymbol{\lambda}, \nabla \boldsymbol{L} - \boldsymbol{M});$$

Where

$$\Phi(\boldsymbol{\lambda}, \nabla \boldsymbol{L} - \boldsymbol{M}) = \tfrac{\mu}{2} \|\nabla \boldsymbol{L} - \boldsymbol{M}\|_2^2 + \langle \boldsymbol{\lambda}, \nabla \boldsymbol{L} - \boldsymbol{M} \rangle, \quad (11)$$

where $\langle \cdot,\cdot \rangle$ represents matrix element-wise multiplication. $\boldsymbol{\lambda}$ is the Lagrangian multiplier, and μ is a positive penalty scalar which controls the speed of convergence to the solution. The three variables ($\boldsymbol{L}$, $\boldsymbol{M}$, and $\boldsymbol{\lambda}$) in (11) should be solved. In the augmented Lagrangian method, the problem can be solved by iteratively updating one of three variables at a time while fixing the others. Therefore, the optimization problem is divided into three sub-problems as follows:

1) $\boldsymbol{L}$ *sub-problem*: Considering all the terms involving $\boldsymbol{L}$ in (11), the $\boldsymbol{L}$ sub-problem at j^{th} iteration is formulated as:

$$\boldsymbol{L}^{(j+1)} = \arg\min_{\boldsymbol{L}} \|\hat{\boldsymbol{L}} - \boldsymbol{L}\|_2^2 + \Phi\left(\boldsymbol{\lambda}^{(j)}, \nabla \boldsymbol{L} - \boldsymbol{M}^{(j)}\right). \quad (12)$$

By taking the partial derivative of the cost function in (12) in reference to $\boldsymbol{L}$ and equate the derivative result to zero, we have:

$$\boldsymbol{L} = \tfrac{2\hat{\boldsymbol{L}} + \boldsymbol{D}^T(\mu \boldsymbol{M} - \boldsymbol{\lambda})}{2 + \mu \boldsymbol{D}^T \boldsymbol{D}}, \quad (13)$$

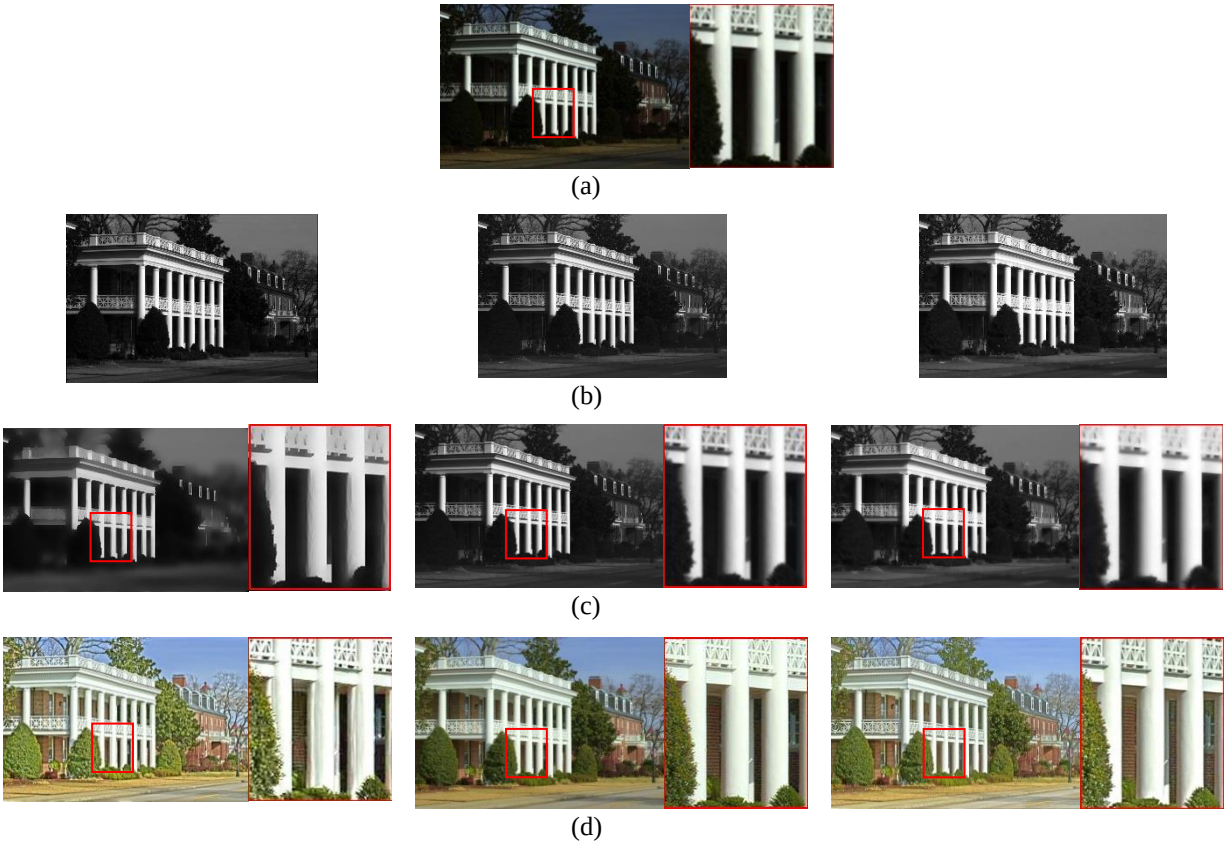

Figure 2: The effect of illumination estimation on the enhanced image. (a) Input image. (b) Initial illumination maps obtained by: LIME [32], NPLIE [36], and proposed algorithm. (c) Their corresponding refined maps. (d) Their corresponding enhanced images.

where $(\cdot)^T$ denotes the transpose operation and $\boldsymbol{D}$ represents the matrix including $\boldsymbol{D}_h$ and $\boldsymbol{D}_v$ which represent the difference along rows and columns, respectively. Using inverse, transpose, and multiplication is computationally expensive for large matrices.
Therefore, $\boldsymbol{L}$ can be computed by utilizing 2D Fast Fourier Transform (FFT) with taking into account the circular boundary conditions as follows:

$$\boldsymbol{L}^{(j+1)} = \mathcal{F}^{-1}\left(\frac{\mathcal{F}(2\hat{\boldsymbol{L}})+\sum_{i\in(h,v)}\overline{\mathcal{F}(\boldsymbol{D}_i)}\mathcal{F}(\mu^j\boldsymbol{M}^j-\lambda^j)}{\boldsymbol{2}+\mu^j\sum_{i\in(h,v)}\overline{\mathcal{F}(\boldsymbol{D}_i)}\circ\mathcal{F}(\boldsymbol{D}_i)}\right), \quad (14)$$

where $\mathcal{F}(\cdot)$, $\bar{\mathcal{F}}(\cdot)$, and $\mathcal{F}^{-1}(\cdot)$ represent the forward, complex conjugate, and the inverse of 2D FFT operations, respectively. $\boldsymbol{2}$ is a matrix in which its size is the same to the image size and all its elements equal 2.

2) $\boldsymbol{M}$ *sub-problem*: By considering all the terms involving $\boldsymbol{M}$ in (11), the $\boldsymbol{M}$ sub-problem at j^{th} iteration is obtained by:

$$\boldsymbol{M}^{(j+1)} = \arg\min_{\boldsymbol{M}} \alpha\|\nabla\boldsymbol{I}_m - \boldsymbol{M}\|_2^2 + \beta\|\boldsymbol{T}\circ\boldsymbol{M}\|_1 + \frac{\mu}{2}\|\nabla\boldsymbol{L} - \boldsymbol{M}\|_2^2 + \langle\boldsymbol{\lambda}, \nabla\boldsymbol{L} - \boldsymbol{M}\rangle. \quad (15)$$

This sub-problem is solved via taking the derivative of (15) in reference to $\boldsymbol{M}$ and equate its result to 0, $\boldsymbol{M}$ is obtained as:

$$\boldsymbol{M} = \frac{2\alpha\nabla\boldsymbol{I}_m+\mu\nabla\boldsymbol{L}+\boldsymbol{\lambda}}{(2\alpha+\mu)} - \frac{\beta\boldsymbol{T}}{(2\alpha+\mu)}. \quad (16)$$

Computing $\boldsymbol{M}$ using (16) may result in negative pixel values in $\boldsymbol{M}$ which is normalized to deal with these negative values. Therefore, shrinkage operation [43] can be used to solve the $\boldsymbol{M}$ sub-problem as:

$$\boldsymbol{M}^{(j+1)} = \boldsymbol{S}_{\frac{\beta\boldsymbol{T}}{(2\alpha+\mu^j)}}\left[\frac{2\alpha\nabla\boldsymbol{I}_m+\mu\nabla\boldsymbol{L}^{(j+1)}+\lambda^j}{(2\alpha+\mu^j)}\right], \quad (17)$$

where $\boldsymbol{S}_{e>0}[\cdot]$ represents the shrinkage operation which is defined as:

$$\boldsymbol{S}_e[u] = sgn(u)\max(|u| - e, 0). \quad (18)$$

The shrinkage operation is performed on the elements of u.

3) $\boldsymbol{\lambda}$ *and* μ *sub-problem*: the values of $\boldsymbol{\lambda}$ and μ are updated via these equations:

$$\boldsymbol{\lambda}^{(j+1)} = \boldsymbol{\lambda}^{(j)} + \mu^{(j)}(\nabla\boldsymbol{L}^{(j+1)} - \boldsymbol{M}^{(j+1)});$$

$$\mu^{(j+1)} = \mu^{(j)}\eta, \eta > 1. \quad (19)$$

To obtain the optimal solution from this iterative algorithm, the maximum number of iterations (j_0) is set to 25.

Gamma correction is then applied on the refined illumination map $\boldsymbol{L}$ to enhance its contrast and consequently improve the visibility of the enhanced result. The gamma-corrected illumination map $\boldsymbol{L}_f$ is obtained as:

$$\boldsymbol{L}_f = \boldsymbol{L}^{\gamma}. \quad (20)$$

Finally, the scene reflectance $\boldsymbol{R}$ which represents the enhanced image is obtained by:

$$\boldsymbol{R} = \boldsymbol{I} \oslash \boldsymbol{L}_f. \quad (21)$$

Algorithm 1 summarizes the steps of the proposed SPLIE algorithm. The effect of estimating the initial illumination using LIME [32], NPLIE [36] and the proposed algorithm on the enhanced images is demonstrated in Figure 2. LIME, NPLIE and the proposed algorithm (SPLIE) used the Max-RGB, structure-aware and proposed fusion-based algorithm for estimating the initial illumination map. As shown in Figure 2(b), the initial illumination map produced by the proposed fusion-based algorithm contains more structural details than that produced by LIME and NPLIE. Consequently, using this estimated initial illumination map for solving a multi-objective optimization problem limits the smoothing effect in structural details and results in textural smoothening in the refined illumination map which is clear in the enlarged red bounded boxes in Figure 2(c). Thus, as shown in Figure 2(d) the enhanced image by the proposed SPLIE algorithm contains more structural details with fewer color distortion and artifacts than that produced by LIME and NPLIE.

Algorithm 1 The proposed SPLIE algorithm.

Input: Low-light image $\boldsymbol{I}$.

Initialization: Constructing weight $\boldsymbol{T}$ using (8),
$j = 0$, $\boldsymbol{L}^{(0)} = 0$, $\boldsymbol{M}^{(0)} = \boldsymbol{\lambda}^{(0)} = 0$.

Step1: Estimate initial illumination map $\hat{\boldsymbol{L}}$ of $\boldsymbol{I}$ using (6).

Step2: Refine illumination map $\boldsymbol{L}$ based on $\hat{\boldsymbol{L}}$ via optimization function using (10),
while $j < j_0$ **do**
Update $\boldsymbol{L}^{(j+1)}$ using (14);
Update $\boldsymbol{M}^{(j+1)}$ using (17);
Update $\boldsymbol{\lambda}^{(j+1)}$ and $\mu^{(j+1)}$using (19);
$j = j + 1$;
end

Step3: Apply Gamma correction on $\boldsymbol{L}$ using (20).

Step4: Obtain the enhanced image using (21).

Output: Scene reflectance $\boldsymbol{R}$ which represents the enhanced image.

4. EXPERIMENTAL RESULTS

The performance of proposed SPLIE algorithm was tested in this section using five low-light image datasets [11, 28, 32, 44, 45]. The datasets contain images with various illumination conditions and sizes. The proposed algorithm was compared quantitatively and qualitatively with several state-of-the-art enhancement algorithms, such as simultaneous reflection and illumination estimation (SRIE) [22], low-light image enhancement (LIME) [32], robust Retinex model (ROR) [24], low-light enhancement using camera response (LECARM) [33], nature preserving low-light image enhancement (NPLIE) [36], and zero-reference deep curve estimation (Zero-DCE) [16]. All the experiments were performed using Matlab R2018a on a computer with 4G RAM and an Intel Pentium Processor of 2.16 GHz.

4.1. Parameter Analysis

In the proposed algorithm, there are two regularization parameters (α and β) which control the structural details and smoothening of textural details respectively and hence affect its performance. It was found experimentally that the values of these parameters are in the range of (0, 1) [36]. According to the multi-objective optimization problem in (7), it does not make any sense to consider α and β as negative values. In addition, if the value of either α or β is more than 1, one of structural or textural details will be dominant. For example, if the value of α is more than 1, this will give more dominance to structural details. Furthermore, the textural details may be enhanced while capturing the structural details which may produce unnatural enhanced images. In the same way, if the value of β is more than 1, this will give more dominance to textural details. In addition, the structural details may be smoothed as well while smoothing the textural details which may over-smoothen the refined illumination. Therefore, the values of α and β are considered to be in the range of (0, 1) to avoid the dominance of the term related to any of these regularization parameters. Many experiments on several images were performed and it was found that the optimal values of α and β that achieve good enhancement results were 0.5 and 0.08, respectively. These values make a good balance between achieving the required smoothening of textural details and preserving the structural details. In the case of α=0.5, the structural details are preserved without over-enhancing the textural details. However, when the value of α is more than 0.5, the textual details are preserved with the structural details. On contrast, when the value of α is less than 0.5, the structural details are not preserved sufficiently. In the case of β= 0.08, the textural details are smoothed without losing structural details. However, when the value of β is more than 0.08, the structural details are smoothed along

(a) (b) (c) (d)

Figure 3: The effect of regularization parameters on illumination map estimation. (a) α=0.5, β =0.08; (b) α=0.5, β =1; (c) α=1, β =0.08; (d) α=1, β =1.

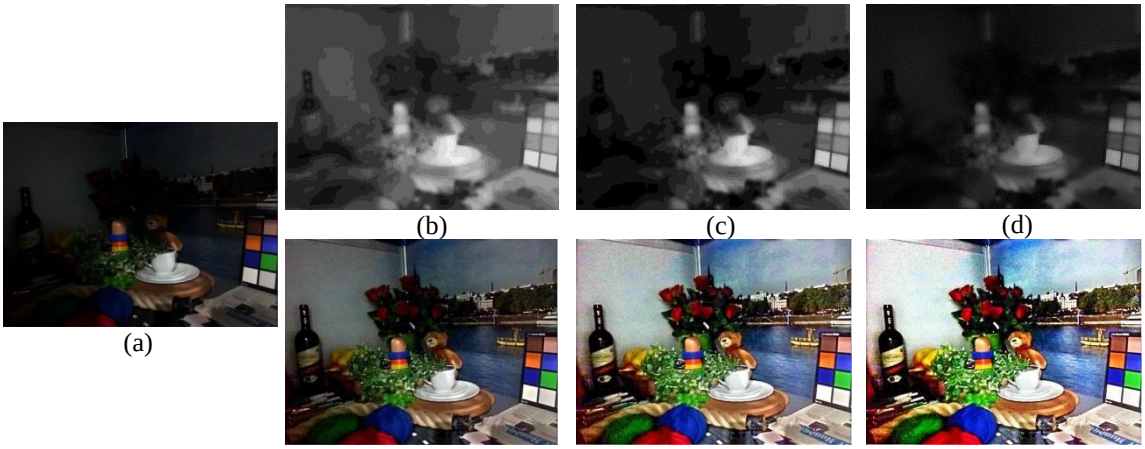

(a) (b) (c) (d) (e) (f) (g)

Figure 4: The results of gamma correction for the illumination map. (a) Input image. (b)-(d) The corrected illumination maps with γ=0.6, γ=0.9, and γ=1. (e)-(g) Their corresponding recovered images.

with the textural details. On the other hand, when the value of β is less than 0.08, the textural details are not smoothed sufficiently. Figure 3 shows the
estimated illumination map for some distinct values of α and β.

The refined illumination map is then enhanced using gamma correction. Figure 4 shows the difference between the results by setting γ to 0.6, 0.9, and 1. It can be observed that at γ=1, the enhanced image looks over-enhanced and unnatural while at γ=0.6, the enhanced image looks slightly dim. Therefore, for the rest experiments, the value of γ was adopted to 0.9 as it produces satisfying and natural results. Moreover, the standard deviation σ in (9) was set to 2 as in [32].

4.2. Qualitative Assessment

In this subsection, several comparisons are given to qualitatively evaluate the proposed SPLIE algorithm performance as compared with SRIE, LIME, ROR, LECARM, NPLIE, and Zero-DCE. Figure 5- Figure 11 show the visual comparison among the enhancement algorithms applied on the low light images in datasets.

Figure 5- Figure 9 show the comparison of enhancement algorithms in different outdoor scenes. It can be observed from these figures that SRIE preserves the naturalness and details of enhanced images, however the brightness of input images is not sufficiently improved by SRIE, and the output images are still dim. On contrast, LIME algorithm achieves a good enhancement in low-light images brightness, nevertheless it suffers from over-enhancement and color saturation in the bright areas which results in distortion on these regions and losing some details in the enhanced image. It is also observed that ROR slightly enhances the input images brightness, however the enhanced image details are over-smoothed which makes the image look unnatural. Although the outputs of LECARM are acceptable, they have a greyish shade which makes the enhanced images appear less exposed. Therefore, the visibility of the enhanced images produced by LECARM needs to be improved. The outputs of NPLIE have some over-enhanced areas in which the details of enhanced images are not clear enough. Furthermore, it is observed that Zero-DCE enhances the input images illumination. Nevertheless, it is unable to recover the true colors and textural details of input images which results in unnatural and pale enhanced images. As shown in Figure 5- Figure 9, the proposed SPLIE algorithm produces satisfying results in different outdoor scenes. It enhances the input low-light images illumination while preserving the structural details and naturalness.

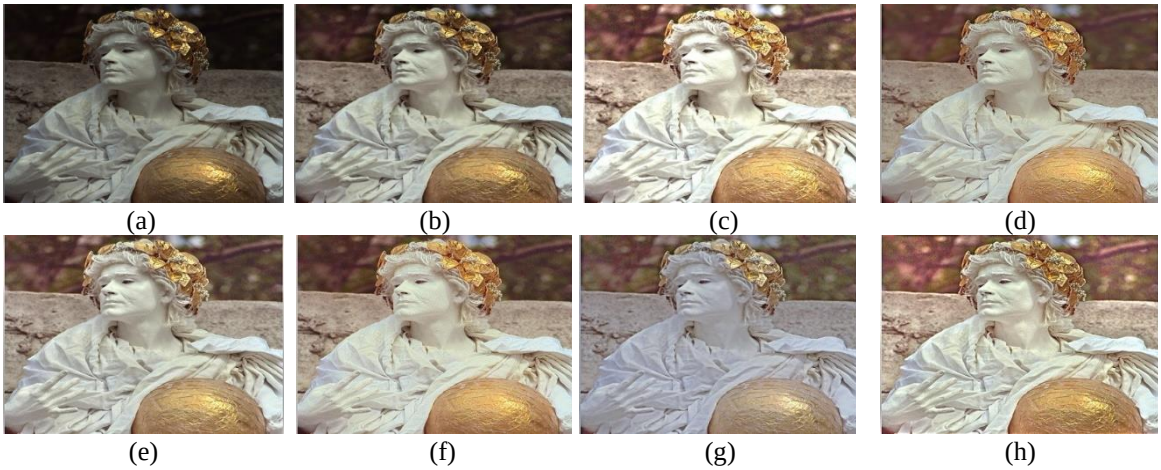

(a) (b) (c) (d)

(e) (f) (g) (h)

Figure 5: The comparison of enhanced images produced by different methods. (a) Input image. (b) SRIE [22]. (c) LIME [32]. (d) ROR [24]. (e) LECARM [33]. (f) NPLIE [36]. (g) Zero-DCE [16]. (h) Proposed SPLIE.

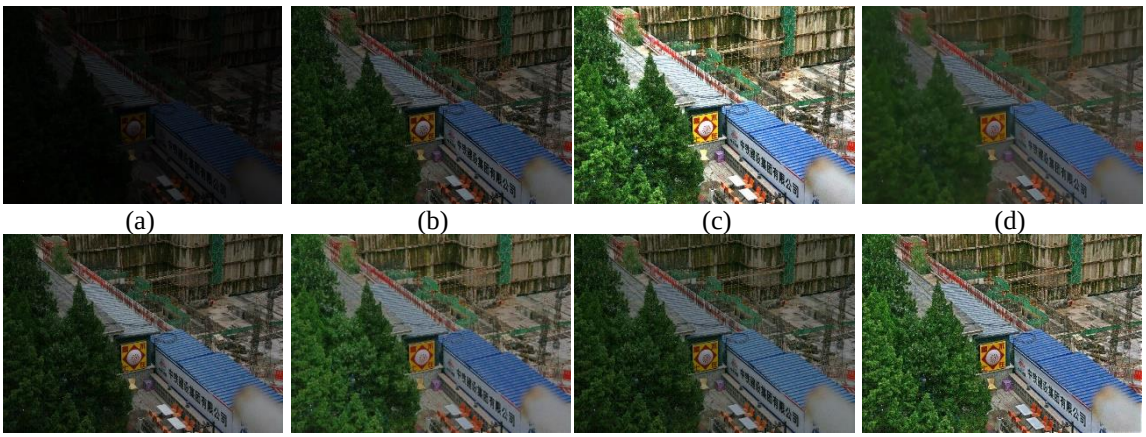

(a) (b) (c) (d)

(e) (f) (g) (h)

Figure 6: The comparison of enhanced images produced by different methods. (a) Input image. (b) SRIE [22]. (c) LIME [32]. (d) ROR [24]. (e) LECARM [33]. (f) NPLIE [36]. (g) Zero-DCE [16]. (h) Proposed SPLIE.

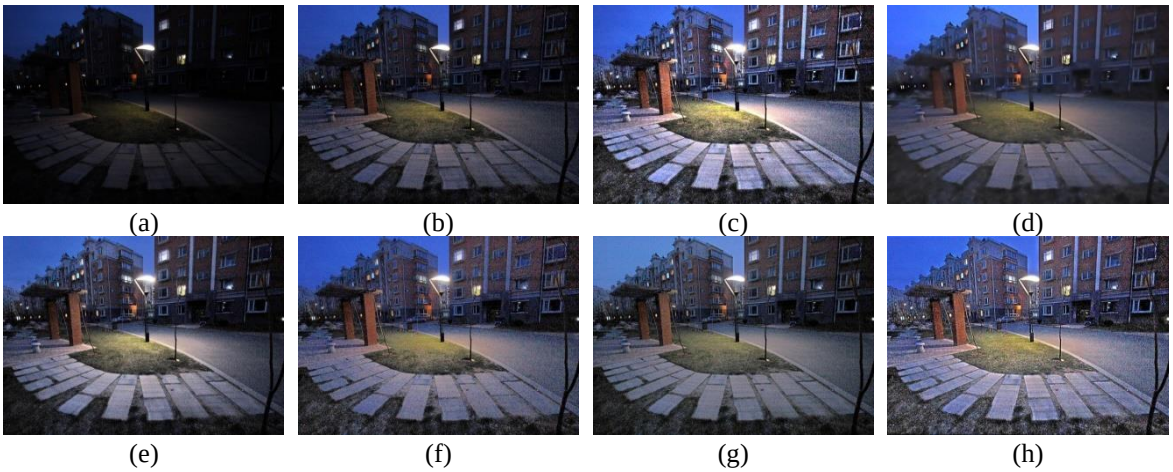

(a) (b) (c) (d)

(e) (f) (g) (h)

Figure 7: The comparison of enhanced images produced by different methods. (a) Input image. (b) SRIE [22]. (c) LIME [32]. (d) ROR [24]. (e) LECARM [33]. (f) NPLIE [36]. (g) Zero-DCE [16]. (h) Proposed SPLIE.

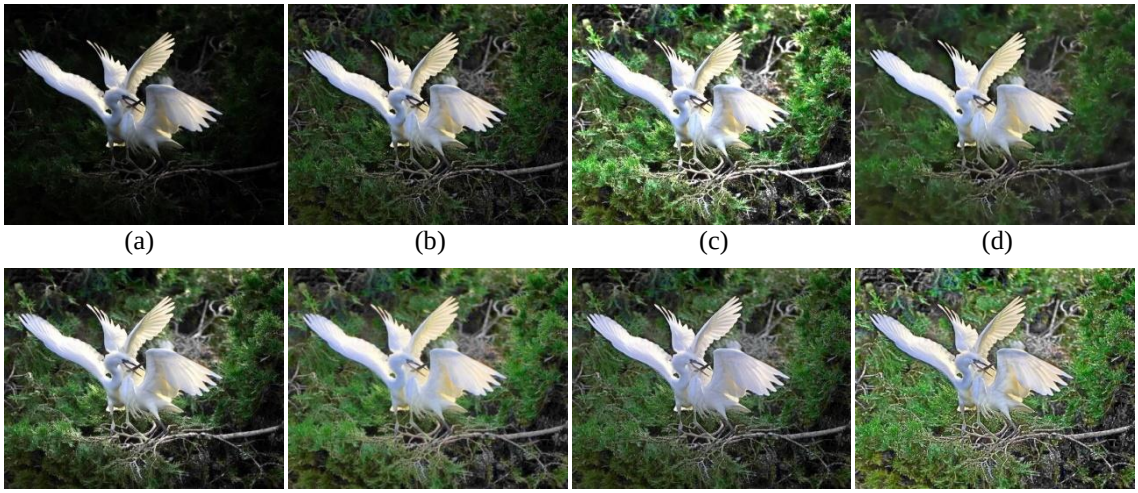

(a) (b) (c) (d)

(e) (f) (g) (h)

Figure 8: The comparison of enhanced images produced by different methods. (a) Input image. (b) SRIE [22]. (c) LIME [32]. (d) ROR [24]. (e) LECARM [33]. (f) NPLIE [36]. (g) Zero-DCE [16]. (h) Proposed SPLIE.

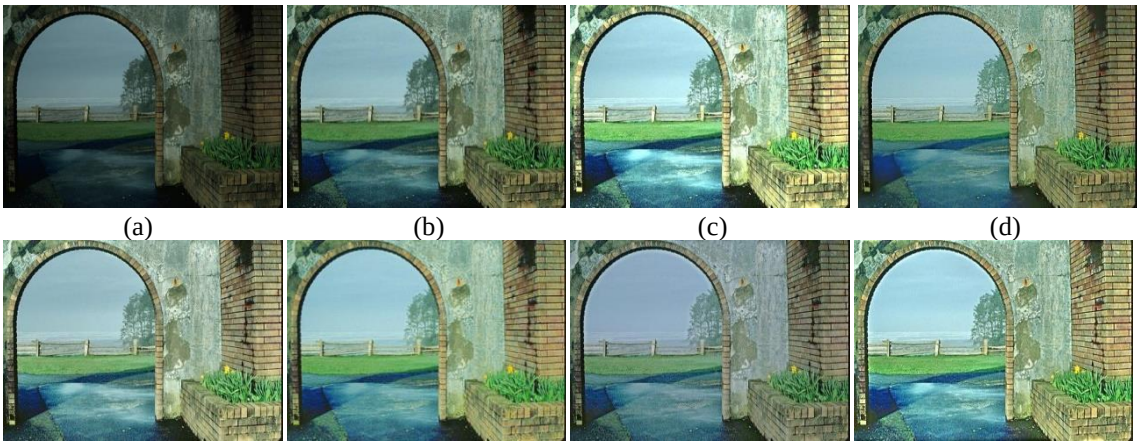

(a) (b) (c) (d)

(e) (f) (g) (h)

Figure 9: The comparison of enhanced images produced by different methods. (a) Input image. (b) SRIE [22]. (c) LIME [32]. (d) ROR [24]. (e) LECARM [33]. (f) NPLIE [36]. (g) Zero-DCE [16]. (h) Proposed SPLIE.

Figure 10 shows the comparison of the enhancement algorithms in different indoor scenes. It can be observed from this figure that the SRIE is unable to maintain the illumination of input images and the improvement in the image quality is not apparent enough whereas LIME shows impressive performance in brightening the dark regions but it may easily over-enhance regions with bright colors. ROR can effectively improve the contrast of weakly illuminated images while suppressing the intensive noise. Nevertheless, the details of the enhanced images are over-smoothed. It can also be observed that LECARM does not improve the brightness of indoor scenes sufficiently. Although NPLIE and Zero-DCE produce pleasing results compared with the other mentioned algorithms, the output of these algorithms look slightly pale with not enough details. The proposed SPLIE algorithm produces promising results and enhance the indoor scenes better than the other enhancement algorithms.

To further clarify the quality difference between the enhanced images generated by SPLIE and the other enhancement algorithms, Figure 11 shows the comparison of enhanced images in local regions. The selected yellow boxes from the input dimmed images shown in Figure 11 (left column) were zoomed-in to clearly demonstrate the enhancement of these local regions by different enhancement algorithms. The zoomed-in patches demonstrate that the proposed SPLIE algorithm generates more clear structural details with fewer color distortion and visual artifacts than the other algorithms. It can be concluded that the SPLIE algorithm

(a) (b) (c) (d) (e) (f) (g) (h)

Figure 10: The comparison of enhancement algorithms in different indoor scenes. (a) Input image. (b) SRIE [22]. (c) LIME [32]. (d) ROR [24]. (e) LECARM [33]. (f) NPLIE [36]. (g) Zero-DCE [16]. (h) Proposed SPLIE.

(a) (b) (c) (d) (e) (f) (g) (h)

Figure 11: The comparison of enhanced images in local regions. (a) Input image. (b) SRIE [22]. (c) LIME [32]. (d) ROR [24]. (e) LECARM [33]. (f) NPLIE [36]. (g) Zero-DCE [16]. (h) Proposed SPLIE.

subjectively achieves better trade-off between the illumination enhancement and preserving the naturalness and structural details of input images than other methods due to using the proposed fusion algorithm in addition to the illumination map refinement.

4.3. Quantitative Assessments

To validate the visual results, the objective evaluation was performed on the results of the enhancement algorithms using non-reference and full reference quality metrics. These quality metrics are the lightness order error (LOE) [28], the discrete entropy (DE) [46], the measure of enhancement (EME) [47], the maximum contrast with minimum artifact (MCMA) [48], peak signal-to-noise ratio (PSNR) [49], and structural similarity index measure (SSIM) [50].

To evaluate the performance in terms of brightness enhancement, the lightness naturalness is measured using LOE metric. It is given as:

$$LOE = \frac{1}{N}\sum_{x=1}^{N}\sum_{y=1}^{N}(U(Z(x), Z(y)) \oplus U(Z_e(x), Z_e(y)). \quad (22)$$

$$U(p,q) = \begin{cases} 1, & \text{if } p \geq q \\ 0, & \text{otherwise} \end{cases}, \quad (23)$$

where $\oplus$ is the XOR operation, N is the pixels number. $Z(x)$ and $Z_e(x)$ denote the maximum values at location x within the RGB color channels of the input low-light image and the enhanced image, respectively. The lower LOE value represents more preservation of lightness order.

Table 1: Quantitative assessment in terms of LOE, DE, EME, and MCMA

Evaluation	SRIE [22]	LIME [32]	ROR [24]	LECARM [33]	NPLIE [36]	Zero-DCE [16]	Proposed SPLIE
LOE [28]	578.06	631.09	717.04	657.23	622.52	670.70	**465.52**
DE [46]	4.86	5.11	4.47	4.88	5.00	4.77	**5.14**
EME [47]	7.89	8.10	5.19	7.23	7.35	6.69	**8.22**
MCMA [48]	0.21	0.13	0.18	0.15	0.15	0.12	**0.11**

To evaluate the details preservation, the information amount in the final enhanced image $\boldsymbol{R}$ is measured using DE metric. It can be calculated by:

$$DE = -\sum_{i=1}^{K} P_i(\boldsymbol{R})\log\left(P_i(\boldsymbol{R})\right), \quad (24)$$

where $P_i(\boldsymbol{R})$ is the occurrence probability of a pixel value i in the image $\boldsymbol{R}$, K denotes the gray levels number. The higher DE value implies that the enhanced image contains more details.

Further, The level of contrast enhancement in the enhanced image $\boldsymbol{R}$ is measured by EME metric. It can be formulated as:

$$EME(\boldsymbol{R}) = \frac{1}{k_1 k_2}\sum_{l=1}^{k_1}\sum_{k=1}^{k_2} 20\, ln\frac{max_{k,l}(\boldsymbol{R})}{min_{k,l}(\boldsymbol{R})}, \quad (25)$$

where $max_{k,l}(\boldsymbol{R})$, and $min_{k,l}(\boldsymbol{R})$ represent the maximum and minimum intensities in each of the enhanced image blocks. High EME value implies that the enhancement algorithm achieves a good contrast improvement.

Moreover, the MCMA metric evaluates the quality of enhancement algorithm relating to the contrast enhancement. It measures the negative impacts that may occur during the enhancement process like, over-enhancement or other artifacts such as, information loss. The MCMA metric can be formulated as:

$$MCMA = \frac{(0.4P_{DRO} - 0.3P_{HSD} - 0.7P_{PU})}{1.4}, \quad (26)$$

where the three parameters, P_{DRO}, P_{HSD}, and P_{PU} are estimated from the enhanced image. These parameters denote the dynamic range occupation (DRO), the histogram shape deformation (HSD), and the pixel uniformity (PU), respectively [48]. Lower MCMA value indicates that the contrast is improved by the enhancement algorithm with minimum artifacts.

Finally, the full reference quality metrics including PSNR and SSIM are utilized to evaluate the similarity between the enhanced images and the corresponding ground truth. PSNR metric measures the enhanced image quality by expressing its distance from the corresponding ground truth. The PSNR metric can be calculated as follows:

$$PSNR = 10\log\left(\frac{{MAX_I}^2}{\frac{1}{m\times n}\sum_{x=1}^{m}\sum_{y=1}^{n}(I_{ref}(x,y) - R(x,y))^2}\right), \quad (27)$$

where MAX_I denotes the image's maximum pixel value. It takes the value of 255 in 8-bit images. $\boldsymbol{I}_{ref}$ and $\boldsymbol{R}$ denote the reference image and the enhanced image of size $m \times n$, respectively. The higher value of PSNR implies a smaller change between the reference and enhanced images which indicates better quality of enhanced image as the image is closer to its corresponding ground truth.

The SSIM metric evaluates the identicality between the enhanced image and its reference image related to the brightness l, contrast c, and structure s. Therefore, the SSIM metric can be calculated as follows [50]:

$$SSIM = F\left[l(I_{ref}, R), c(I_{ref}, R), s(I_{ref}, R)\right]. \quad (28)$$

The higher value of SSIM implies more similar structure between the enhanced image and its reference image.

The efficiency of the proposed SPLIE algorithm is assessed via the quality measures including, LOE, DE, EME, and MCMA. These metrics are used to evaluate the enhanced images from the datasets that have been used. Table 1 clarifies the average LOE, DE, EME, and MCMA measures gained from SPLIE and the other enhancement algorithms. It can be noticed that ROR produces the worst result of LOE, DE, and EME because this method over-smoothes the enhanced image in which the details are not prominent enough and makes the enhanced image looks unnatural. Whereas, SRIE has the highest value of MCMA because this method could not improve the brightness of input images sufficiently and produces enhanced images with visual artifacts.

It is observed that the proposed SPLIE algorithm obtains better results in all measures. It achieves the lowest LOE average value which indicates that SPLIE can recover the low-light images brightness while preserving their naturalness. Furthermore, compared to the other algorithms, SPLIE produces the best scores in terms of DE, EME, and MCMA which implies that the proposed SPLIE algorithm improves the contrast while maintaining the image structural details and reducing the color distortions and artifacts. This improvement is due to using the fusion-based mechanism for estimating the

Table 2: Objective assessment in terms of PSNR and SSIM

Evaluation	SRIE [22]	LIME [32]	ROR [24]	LECARM [33]	NPLIE [36]	Zero-DCE [16]	Proposed SPLIE
PSNR	13.05	16.66	15.60	17.82	17.76	17.37	**18.60**
SSIM	0.61	0.69	0.66	0.71	0.71	0.70	**0.74**

Table 3: The average running time of several low-light image enhancement methods (in seconds)

Evaluation	SRIE [22]	LIME [32]	ROR [24]	LECARM [33]	NPLIE [36]	Zero-DCE [16]	Proposed SPLIE
Time	50.80	3.58	80.70	2.06	15.22	**0.018**	18.29

initial illumination map of input image and using multi-objective function to obtain the refined illumination map.

The full reference metrics including PSNR and SSIM were also used to check the performance of the proposed SPLIE algorithm on LOL dataset [11]. The average PSNR and SSIM measures gained from the proposed SPLIE and the other algorithms are illustrated in Table 2.

It is clear from the table that the proposed algorithm obtains the highest scores of PSNR and SSIM which implies that the enhanced images obtained from the proposed SPLIE algorithm are closer to their reference images than the other enhancement algorithms. It can be concluded that the proposed algorithm outperforms other enhancement algorithms and hence it is effective for the enhancement of low-light images.

4.4. Processing Time

Table 3 illustrates the average processing time of several enhancement algorithms. As shown in the table, the ROR is the slowest algorithm among the other enhancement algorithms. This method requires large computational time due to its consecutive iterations and causes out of memory problems especially in the processing of large size images. Whereas, Zero-DCE has the lowest running time that represents the test phase duration. However, the training time of this method is about 30 minutes [16]. Although the processing time of the proposed algorithm is not the fastest compared to the other enhancement algorithms, it produces the best results in the subjective and objective evaluations.

5. CONCLUSION

In this paper, an effective algorithm was proposed to improve low-light images depending on Retinex model. The key for good recovery of enhanced image is how accurate the illumination map is obtained. Therefore, the proposed algorithm was intended to obtain the optimal illumination map of observed weakly illuminated image. The initial illumination map was obtained using fusion between maximum color channel and bright channel of input image. The optimized illumination was then estimated by refining the initial illumination map using structure-aware smoothing model. The experimental results demonstrated the outperformance of the proposed SPLIE algorithm over the other enhancement algorithms. The proposed algorithm makes the low-light images more visible by enhancing their illumination while avoiding over-enhancement. Furthermore, it weakens the color distortion and halo artifacts while preserving the naturalness and structural details of the enhanced images. Therefore, our proposed SPLIE algorithm can be used to introduce high visibility input images to several computer vision applications, such as traffic monitoring, surveillance systems, remote sensing systems, and medical imaging systems which thus improve the performance of these applications.

Credit Authorship Contribution Statement:

Ghada Sandoub: methodology, software, investigation, writing original draft;

Randa Atta: methodology, conceptualization, writing, editing, reviewing & supervision;

Hesham Arafat Ali: reviewing & supervision;

Rabab Farouk Abdel-Kader: reviewing & supervision.

Declaration of competing Interest

The authors declare that they have no conflicting financial interests or personal relationships that may have influenced the work presented in this article.

References

[1] E. D. Pisano, S. Zong, B. M. Hemminger, et al., "Contrast limited adaptive histogram image processing to improve the detection of simulated speculations in dense mammograms," Journal of Digital Imaging, vol. 11, no. 4, pp. 193–200, 1998.

[2] M. Abdullah-Al-Wadud, M. Kabir, M. Dewan, and O. Chae, "A dynamic histogram equalization for image contrast enhancement," IEEE Transactions on Consumer Electronics, vol. 53, no. 2, pp. 593–600, 2007.

[3] T. Celik, and T. Tjahjadi, "Contextual and variational contrast enhancement," IEEE Transactions on Image Processing, vol. 20, no. 12,

pp. 3431–3441, 2011.

[4] K. Singh, and R. Kapoor, “Image enhancement using exposure based sub image histogram equalization,” Pattern Recognition Letters, vol. 36, no. 15, pp. 10–14, 2014.

[5] A. S. Parihar, and O. P. Verma, “Contrast enhancement using entropy-based dynamic sub-histogram equalization,” IET Image Processing, vol. 10, no. 11, pp. 799 – 808, 2016.

[6] P. P. Banik, R. Saha, and K. Kim, “Contrast enhancement of low-light image using histogram equalization and illumination adjustment,” In Proc. IEEE International Conference on Electronics, Information, and Communication (ICEIC), Honolulu, HI, USA, January 2018, pp. 1-4.

[7] S. F. Tan, and N. A. M. Isa, “Exposure Based Multi-Histogram Equalization Contrast Enhancement for Non-Uniform Illumination Images,” IEEE Access, vol. 7, pp. 70842–70861, 2019.

[8] C. Li, S. Tang, J. Yan, and T. Zhou, “Low-light image enhancement based on quasi-symmetric correction functions by fusion,” Symmetry, vol. 12, no. 9, pp. 1561, 2020.

[9] W. Wang, C. Wei, W. Yang, and J. Liu, “GLADNet: Low-light enhancement network with global awareness,” In Proc. 13th IEEE International Conference on Automatic Face & Gesture Recognition (FG 2018), May 2018, pp. 751-755.

[10] C. Li, J. Guo, F. Porikli, and Y. Pang, “LightenNet: A convolutional neural network for weakly illuminated image enhancement,” Pattern Recognition Letters, vol. 104, pp. 15–22, 2018.

[11] Ch. Wei, W. Wang, W. Yang, and J. Liu, “Deep Retinex decomposition for low-light enhancement,” In Proc. British Machine Vision Conference (BMVC 2018), 2018, pp. 1–12.

[12] R. Wang, Q. Zhang, Ch. Fu, X. Shen, et al., “Underexposed photo enhancement using deep illumination estimation,” In Proc. IEEE Conference on Computer Vision and Pattern Recognition (CVPR), 2019, pp. 6849–6857.

[13] Y. Jiang, X. Gong, D. Liu, Y. Cheng, et al., “EnlightenGAN: Deep light enhancement without paired supervision,” IEEE Transactions on Image Processing, vol. 30, pp. 2340-2349, 2021.

[14] W. Ren, S. Liu, L. Ma, Q. Xu, et al., “Low-light image enhancement via a deep hybrid network,” IEEE Transactions on Image Processing, vol. 28, no. 9, pp. 4364-4375, 2019.

[15] L. Ma, R. Liu, J. Zhang, X. Fan, and Z. Luo, “Learning deep context-sensitive decomposition for low-light image enhancement,” IEEE Transactions on Neural Networks and Learning Systems, 2021.

[16] Ch. Guo, Ch. Li, J. Guo, Ch. Loy, et al., “Zero-reference deep curve estimation for low-light image enhancement,” In Proc. IEEE Conference on Computer Vision and Pattern Recognition (CVPR), 2020, pp. 1777-1786.

[17] E. H. Land, and J. J. McCann, “Lightness and Retinex theory,” Journal of the Optical Society of America, vol. 61, no. 1, pp. 1-11, 1971.

[18] D. J. Jobson, Z. U. Rahman, and G. A. Woodell, “Properties and performance of a centre/surround Retinex,” IEEE Transactions on Image Processing, vol. 6, no. 3, pp. 451–462, 1996.

[19] Z. Rahman, D. J. Jobson, and G. A. Woodell, “Multi-scale Retinex for color image enhancement,” In Proc. IEEE international conference on Image Processing, Lausanne, Switzerland, September 1996, pp. 1003-1006.

[20] D. J. Jobson, Z. Rahman, and G. A. Woodell, “A multiscale Retinex for bridging the gap between color images and the human observation of scenes,” IEEE Transactions on Image Processing, vol. 6, no. 7, pp. 965–976, 1997.

[21] X. Fu, D. Zeng, Y. Haung, et al., “A variational framework for single low light image enhancement using bright channel prior,” In Proc. IEEE Global Conference on Signal and Information Process., Austin, TX, USA, December 2013, pp. 1085-1088.

[22] X. Fu, D. Zeng, Y. Huang, et al., “A weighted variational model for simultaneous reflectance and illumination estimation,” In Proc. IEEE International Conference on Computer Vision and Pattern Recognition (CVPR), 2016, pp. 2782–2790.

[23] Y. Wu, W. Song, J. Zheng, and F. Liu, “A new low light image enhancement based on the image degradation model,” In Proc. 14th IEEE International Conference Signal Processing (ICSP), August 2018, pp. 379–383.

[24] M. D. Li, J. Y. Liu, W. H. Yang, X. Y. Sun, and Z. M. Guo, “Structure revealing low-light image enhancement via robust Retinex model,” IEEE Transactions on Image Processing, vol. 27, no. 6, pp. 2828-2840, 2018.

[25] C. Dai, M. Lin, J. Wang, and X. Hu, “Dual-purpose method for underwater and low-light image enhancement via image layer separation,” IEEE Access, vol. 7, pp. 178685-178698, 2019.

[26] X. Ren, W. Yang, W. H. Cheng, and J. Liu, “LR3M: Robust low-light enhancement via low-rank regularized Retinex model,” IEEE Transactions on Image Processing, vol. 29, pp. 5862-5876, 2020.

[27] L. Wang, Q. Ge, W. Shao, P. Wu, and H. Deng,

"Structure-based low-rank Retinex model for low-light image enhancement," In Proc. Twelfth International Conference on Graphics and Image Processing (ICGIP), International Society for Optics and Photonics, vol. 11720, pp. 1172016, 2021.

[28] J. Zheng, S. Wang, H. M. Hu, et al., "Naturalness preserved enhancement algorithm for non-Uniform illumination images," IEEE Transactions on Image Processing, vol. 22, no. 9, pp. 3538–3547, 2013.

[29] S. Sun, and X. Guo, "Image enhancement using bright channel prior," In Proc. IEEE International Conference on Industrial Informatics Computing Technology, Intelligent Technology, Industrial Information Integration (ICIICII), Wuhan, China, December 2016, pp. 83-86.

[30] L. Chen, W. Sun, and J. Feng, "A fast image enhancement algorithm using bright channel," Intelligent Data Analysis and Its Applications, Volume II, Springer, Cham, vol. 2, pp. 565-574, 2014.

[31] X. Fu, D. Zeng, Y. Huang, et al., "A fusion-based enhancing method for weakly illuminated images," Signal Processing, vol. 129, pp. 82-96, 2016.

[32] Y. Li, X. Guo, and H. Ling, "Lime: Low-light image enhancement via illumination map estimation," IEEE Transactions on Image Processing, vol. 26, no. 2, pp. 982-993, 2017.

[33] Y. Ren, Z. Ying, T. H. Li, et al., "LECARM: Low-light image enhancement using camera response model," IEEE Transactions on Circuits and Systems for Video Technology, vol. 29, no. 4, pp. 968 – 981, 2018.

[34] Y. Wu, J. Zheng, W. Song, et al., "A novel low light image enhancement based on non-uniform illumination prior model," IET Image Processing, pp.1-10, 2019.

[35] Q. Zhang, Y. Nie, and W. S. Zheng, "Dual illumination estimation for robust exposure correction," Computer Graphics Forum, vol. 38, no. 7, pp. 243–252, 2019.

[36] K. Singh, and A. S. Parihar, "Illumination Estimation for Nature Preserving low-light image enhancement," TechRxiv. Preprint. https://doi.org/10.36227/techrxiv.12236780.v1, (2020) Accessed July 2020

[37] X. Feng, J. Li, Z. Hua, and F. Zhang, "Low-light image enhancement based on multi-illumination estimation," Applied Intelligence, pp.1-21, 2021.

[38] E. Land. The Retinex theory of color vision. Scientific American, vol. 237, no. 6, pp. 108-128, 1977.

[39] G. Sandoub, R. Atta, H.A. Ali, and R.F. Abdel-Kader, "A low-light image enhancement method based on bright channel prior and maximum color channel," IET Image Processing, vol. 15, no. 8, pp. 1759-1772, 2021.

[40] S. Sridhar, "*Digital image processing*," Oxford University Press, 2011.

[41] L. Xu, Q. Yan, Y. Xia, and J. Jia, "Strucutre extraction from texture via relative total variation," TOG, vol. 31, no. 6, pp. 139:1–139:10, 2013.

[42] Y. Wang, W. Yin, and J. Zeng, "Global convergence of admm in nonconvex nonsmooth optimization," Journal of Scientific Computing, vol. 78, no. 1, pp. 29–63, 2019.

[43] R. Chartrand, "Shrinkage mappings and their induced penalty functions," In Proc. IEEE International Conference on Acoustics, Speech and Signal Processing (ICASSP), Florence, 2014, pp. 1026-1029.

[44] NASA. Retinex image processing. 2001, https://dragon.larc.nasa.gov/Retinex/pao/news/, Accessed February 2019

[45] V. Vonikakis, "A collection of the most challenging cases," https://sites.google.com/site/vonikakis/datasets/challenging-dataset-for-enhancement, Accessed February 2019

[46] C. E. Shannon, "A mathematical theory of communication," The Bell System Technical Journal, vol. 27, pp. 379–423, 623–656, 1948.

[47] S. Agaian, B. Silver, and K. Panetta, "Transform coefficient histogram based image enhancement algorithms using contrast entropy," IEEE Transactions on Image Processing, vol. 16, no. 3, pp. 741–758, 2007.

[48] M. Abdoli, F. Nasiri, P. Brault, et al., "Quality assessment tool for performance measurement of image contrast enhancement methods," IET Image Processing, vol. 13, no. 5, pp. 833-842, 2019.

[49] S.S. Colores, E. C. Yepez, J. M. R. Arreguin, et al., "A fast image dehazing algorithm using morphological reconstruction," IEEE Transactions on Image Processing, vol. 28, no. 5, pp. 2357-2366, 2019.

[50] Z. Wang, A. Bovik, H. Sheikh, and E. Simoncelli, "Image quality assessment: From error visibility to structural similarity," IEEE Transactions on Image Processing, vol. 13, no. 4, pp. 600-612, 2004.